

Exploring Spin AGP Ansatzes for Strongly Correlated Spin Systems

Zhiyuan Liu,¹ Fei Gao,¹ Guo P. Chen,² Thomas M. Henderson,^{1,2} Jorge Dukelsky,³ and Gustavo E. Scuseria^{1,2}

¹*Department of Physics and Astronomy, Rice University, Houston, TX 77005-1892*

²*Department of Chemistry, Rice University, Houston, TX 77005-1892*

³*Instituto de Estructura de la Materia, IEM-CSIC, Serrano 123, 28006 Madrid, Spain*

(Dated: March 10, 2023)

The antisymmetrized geminal power (AGP), a wave function equivalent to number-projected Hartree-Fock-Bogoliubov (HFB), has proven to be an excellent reference for strong pairing interactions. Several correlation methods have also been applied on top of AGP. In this work, we show how AGP can also be applied to spin systems by simply basing its formulation on a spin $su(2)$ algebra. We here implement spin AGP and spin AGP-based correlation techniques on the XXZ and $J_1 - J_2$ Heisenberg models, both in 1 and 2 dimensions. Our results indicate that AGP is a promising starting point for modeling spin systems.

I. INTRODUCTION

Model spin Hamiltonians provide valuable insight into magnetic materials, high-temperature superconductors, and biochemical processes such as nitrogen fixation [1–3]. They are also important for the study of quantum sensors, cold atoms in optical lattices, and fault-tolerant quantum computers [4–6]. These model Hamiltonians capture diverse physical phenomena without the details of a fully *ab initio* description. Nevertheless, with a few exceptions [7], lattice models of spin systems beyond one-dimension are not exactly solvable, and we have to resort to approximate numerical methods.

Here we focus on the ground states of spin lattice models, whose computation is already challenging due to various quantum phases that arise from different interaction strengths [1, 8–12]. Particularly, analogous to Hartree-Fock in electronic structure theory, spin wave functions based on a single spin configuration are inadequate in the strongly correlated regime [13, 14]. However, our recent work suggests that methods in electronic structure theory can be useful for studying spins if they are mapped to fermions without constraints [15].

The antisymmetrized geminal power (AGP) wave function [16, 17] has been shown to be a good starting point for certain strongly correlated problems. When correlated with configuration interaction (CI) or coupled cluster (CC) theory [18, 19], AGP yields quite accurate results for the reduced Bardeen-Cooper-Schrieffer (BCS) Hamiltonian, which models the kinds of strong correlations seen in conventional superconductors [20, 21].

Though AGP was originally developed for paired fermionic systems, the pairing algebra generators satisfy the same $su(2)$ algebra as do spin operators. Inspired by Anderson’s resonating valence bond theory which was applied to study both the Heisenberg model and Hubbard model [22, 23], we propose to treat spin systems via AGP. Our results suggest that spin AGP, particularly once correlated, is a computationally affordable technique which can accurately describe the ground states of strongly correlated spin systems.

II. THEORY

A. Antisymmetrized Geminal Power

The central concept of AGP [16, 17] is the geminal, a two-electron wave function created by a geminal creation operator

$$\Gamma^\dagger = \frac{1}{2} \sum_{1 \leq p, q \leq 2M} \eta_{pq} c_p^\dagger c_q^\dagger, \quad (1)$$

where η is antisymmetric, c_p^\dagger is the fermion creation operator for spinorbital p , and indices p, q run over all $2M$ spinorbitals. An AGP state with $2N$ electrons is created by occupying the same geminal N times:

$$|\text{AGP}\rangle = \frac{1}{N!} (\Gamma^\dagger)^N |-\rangle, \quad (2)$$

where $|-\rangle$ is the physical vacuum.

In practice, it is more convenient to work in the natural orbital basis of the geminal, where η is quasideagonal [24],

$$\eta = \bigoplus_{p=1}^M \begin{pmatrix} 0 & \eta_p \\ -\eta_p & 0 \end{pmatrix}, \quad (3)$$

displaying a pairing scheme of the spinorbitals [19]. In this basis, we can write

$$\Gamma^\dagger = \sum_{p=1}^M \eta_p P_p^\dagger, \quad (4)$$

in which we have defined

$$P_p^\dagger = c_p^\dagger c_{\bar{p}}^\dagger \quad (5)$$

and have reindexed the fermion creation operators by p and its paired companion \bar{p} , where p enumerates all M pairs. The AGP then assumes the form of an elementary symmetric polynomial:

$$|\text{AGP}\rangle = \sum_{1 \leq p_1 < \dots < p_N \leq M} \eta_{p_1} \dots \eta_{p_N} P_{p_1}^\dagger \dots P_{p_N}^\dagger |-\rangle. \quad (6)$$

Because AGP is equivalent to number-projected Hartree-Fock-Bogoliubov (HFB) [25] or number-projected BCS in the natural orbital basis, it can be optimized with mean-field cost of $\mathcal{O}(M^3)$ [26, 27], and its variationally optimized result is guaranteed to be at least as good as Hartree-Fock, which is just a special case of AGP in which only N of the η 's are non-zero.

In this work, we will not worry about the magnitude of the AGP wave function, which can be normalized by multiplying all the eta's by the same constant.

B. AGP for Spin Systems

The pair creation operator P_p^\dagger and its adjoint P_p , together with the number operator

$$N_p = c_p^\dagger c_p + c_{\bar{p}}^\dagger c_{\bar{p}}, \quad (7)$$

close the the $su(2)$ commutation algebra:

$$[P_p, P_q^\dagger] = \delta_{pq} (1 - N_p), \quad (8a)$$

$$[N_p, P_q^\dagger] = 2 \delta_{pq} P_p^\dagger. \quad (8b)$$

Following Anderson [28], we can relate the AGP commutation algebra to the spin- $\frac{1}{2}$ $su(2)$

$$[S_p^+, S_q^-] = 2 \delta_{pq} S_p^z, \quad (9a)$$

$$[S_p^z, S_q^+] = \delta_{pq} S_p^+. \quad (9b)$$

Comparing with Eqns. (8), we see that by the bijective mapping

$$S_q^+ \leftrightarrow P_q^\dagger, \quad (10a)$$

$$S_q^- \leftrightarrow P_q, \quad (10b)$$

$$S_q^z \leftrightarrow \frac{N_q - 1}{2}, \quad (10c)$$

we can simply transcribe any expressions for standard AGP matrix elements in the zero seniority [29] fermion space, where all electron are paired, to those for spin AGP (sAGP for short), and can readily generalize any of the techniques we have introduced for the correlation of AGP to sAGP [18, 19, 27, 30, 31]. In the standard pairing AGP case, the vacuum is annihilated by P_p for all p , and the corresponding state annihilated by S_p^- for all p is the spin vacuum state $|\downarrow\rangle$ in which every spin is aligned along the \downarrow direction. The sAGP wave function is thus

$$|\text{sAGP}\rangle = \frac{1}{N!} (\Gamma^\dagger)^N |\downarrow\rangle, \quad (11a)$$

$$\Gamma^\dagger = \sum_p \eta_p S_p^+, \quad (11b)$$

where we have a total of N \uparrow -spins and $(M - N)$ \downarrow -spins, so

$$\langle \text{sAGP} | S^z | \text{sAGP} \rangle = N - \frac{M}{2}. \quad (12)$$

At half filling ($N = M/2$) the sAGP wave function is magnetically neutral.

Incidentally, the inverse mapping of Eqns. (10) has been used to implement quantum computing algorithms for the standard AGP [32, 33].

We have noted that standard AGP is equivalent to number-projected BCS, which suggests that there should be an equivalent projected mean-field understanding of sAGP. This is indeed the case: sAGP is simply the S^z -projected spin BCS state, where the spin BCS (sBCS) is defined as

$$|\text{sBCS}\rangle = \prod_{p=1}^M (1 + \eta_p S_p^+) |\downarrow\rangle, \quad (13)$$

in analogy with the standard BCS given in terms of pairing operators P_p^\dagger and the physical vacuum. When the spin problem is mapped to fermions, spin BCS corresponds to generalized Hartree-Fock (GHF) in which the spinorbitals break not only S^2 but also S^z symmetry [34–36].

In this work, in which we specialize to spin Hamiltonians, the GHF wave function has seniority symmetry dictated by the spins, and one could think of sAGP as an S^z -projected general spin product state. Since we are concerned with spin systems in this paper, we will use AGP and sAGP interchangeably in the following.

III. APPLICATIONS

We benchmark spin AGP on two families of spin lattice systems, the XXZ and J_1 - J_2 Heisenberg models [1]. The former captures anisotropic interactions, while the latter includes interactions beyond nearest neighbors.

We focus predominantly on the nearest-neighbor XXZ model. We start with the one-dimensional (1D) case as a prototypical example as it illustrates the most important features of sAGP and is exactly solvable via Bethe ansatz [37]. We then discuss various two-dimensional (2D) XXZ lattices as well as the J_1 - J_2 square lattice, which are not integrable in general.

A. The One-Dimensional XXZ Model

The XXZ Hamiltonian is written as

$$H_{\text{XXZ}} = J \sum_{\langle pq \rangle} (S_p^x S_q^x + S_p^y S_q^y + \Delta S_p^z S_q^z) \quad (14a)$$

$$= J \sum_{\langle pq \rangle} \left[\frac{1}{2} (S_p^+ S_q^- + S_p^- S_q^+) + \Delta S_p^z S_q^z \right], \quad (14b)$$

where p and q index lattice sites and the notation $\langle pq \rangle$ restricts the summation over p and q to nearest neighbors. Generally speaking, we take $J = 1$ so that the system is antiferromagnetic when $\Delta > 1$.

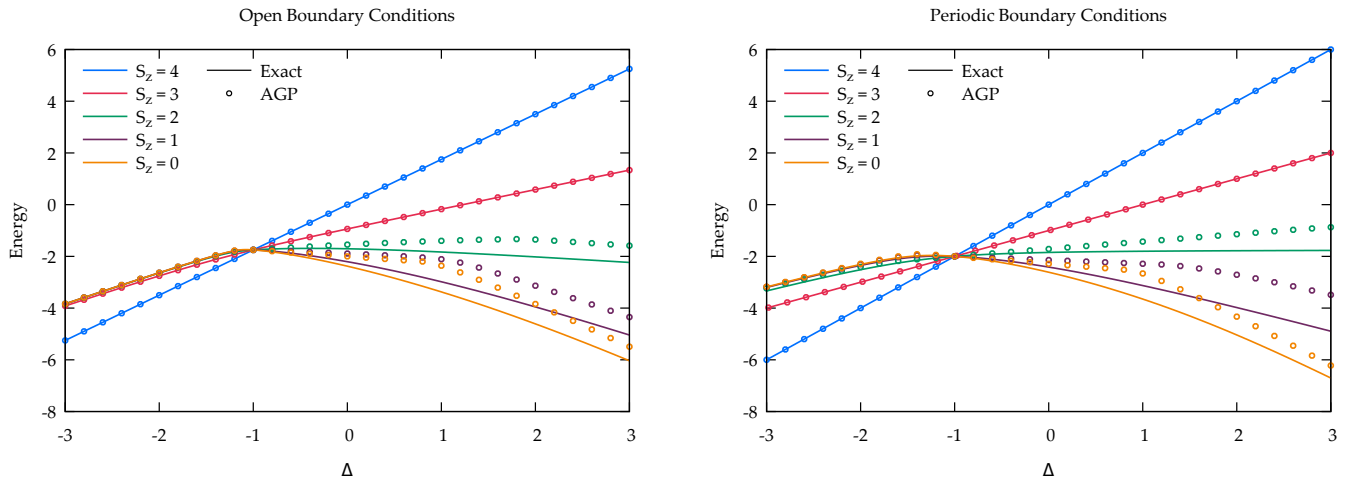


FIG. 1. Energies in the 8-site 1D XXZ Hamiltonian for different S^z sectors and open boundary conditions (left panel) or periodic boundary conditions (right panel). We compare the exact results (lines) against the mean-field optimized sAGP (points). Different colors correspond to different S^z sectors. Spin AGP is very accurate for $\Delta < -1$ and exact for all S^z sectors at $\Delta = -1$.

In the 1D case, sites p and q are nearest neighbors if $|p - q| = 1$. With $J > 0$, it exhibits a Néel antiferromagnetic phase for $\Delta \gtrsim 1$ and a ferromagnetic phase for $\Delta \lesssim -1$. In the interval region, $|\Delta| \lesssim 1$, the system is in the XY phase characterized by gapless excitations and long range correlations [1]. While the ferromagnetic and antiferromagnetic phases are fairly simple to describe, the XY phase is much more complicated, and methods based on a single spin configuration struggle [13, 14]. Spin AGP, however, is exact at $\Delta = -1$, which gives us hope that it will be able to accurately describe this challenging phase as Δ progresses from -1 to $+1$.

1. Energies for Different S^z Sectors

Let us start with an overview of the exact and sAGP ground state energies for different S^z quantum numbers and different values of Δ , as shown in Fig. 1. For $\Delta < -1$, the exact ground state occurs when all the spins are aligned, i.e., at $S^z = \pm M/2$. For $\Delta > -1$, the exact ground state is instead $S^z = 0$. At $\Delta = -1$, the different S^z sectors are exactly degenerate. Spin AGP is exact at $\Delta = -1$ for all S^z sectors and is highly accurate for $\Delta < -1$. For $\Delta > -1$, sAGP is exact for $N = 0$ and $N = 1$, but shows larger error as we approach half-filling ($S^z = 0$).

2. Bimodal Extreme AGP

We now turn to the nature of the sAGP ground state. We find that η values on adjacent sites have opposite signs, for all values of Δ . When Δ is large and negative, the η values on the left (or right) half of sites of the lattice

are large in magnitude, and on the other half are small. Larger $|\eta_p|$ correspond to larger $\langle S_p^z \rangle$; thus, the fact that the large $|\eta|$ values localize on the left (or right) side of lattice means that the \uparrow spins localize on this side, i.e, we have a 2-block ferromagnetic solution. Due to the breaking of inversion lattice symmetry, \uparrow spins can either localize on the left half of sites or right, corresponding to two degenerate states. On the other hand, when Δ is large and positive, alternating sites exhibit a pattern of large and small $|\eta|$, corresponding to a Néel arrangement of spins. These observations are exemplified by the 8-site XXZ chain with open boundary conditions and $S^z = 0$, whose η values are depicted in Fig. 2.

The more interesting region is of course when $-1 \lesssim \Delta \lesssim 1$, and particularly at $\Delta = -1$ where sAGP is exact. In this region, the sAGP wave function is what we refer to as *bimodal extreme*, for which we can choose $\eta = (1, -1, 1, -1 \dots)$, as can be seen from Fig. 2. An AGP is extreme when all η values are the same in magnitude, which corresponds to each site having equal $\langle S^z \rangle$. We refer to the AGP as bimodal when the η 's take on two values, in this case ± 1 . This bimodal extreme sAGP is the exact ground state wave function for $\Delta = -1$ and is the lowest energy sAGP state throughout this XY phase. Note that extreme AGP also has a place in the reduced BCS Hamiltonian $H = \sum_p \epsilon_p N_p - G \sum_{pq} P_p^\dagger P_q$, where, as the interaction strength G goes to infinity, all AGP η approach the same value [18], exhibiting a unimodal extreme AGP.

These features of the sAGP ground state are observed across various lengths of the XXZ chain and S^z values, and for both periodic boundary conditions (PBC) and open boundary conditions (OBC). We also note that bimodal extreme AGP is always a stationary point of the energy, and the points at which the η values begin to

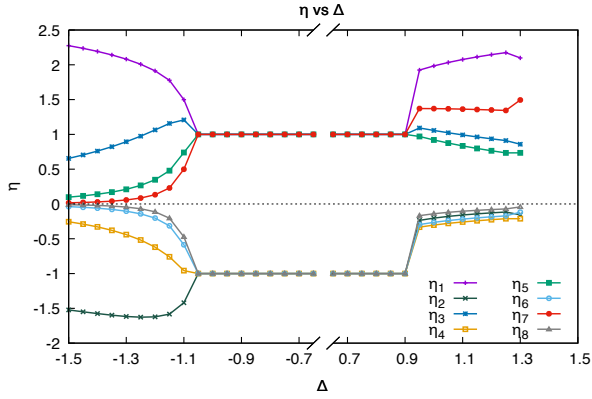


FIG. 2. The AGP geminal coefficient η as a function of Δ for the 8-site XXZ Heisenberg model with open boundary conditions and $S^z = 0$. For $-1 \lesssim \Delta \lesssim 1$ the η values are independent of Δ , and $-0.6 < \Delta < 0.6$ has been omitted from the plot. We order the sites from left to right as η_1 to η_8 .

change occur when it is no longer the lowest energy solution.

3. Spin $su(2)$ Algebras and Multimodal Extreme AGPs

The bimodal extreme AGP mentioned above is just a special case of multimodal extreme AGPs, all of which can be formed from collective spin operators which realize a collective $su(2)$ algebra:

$$K_k^\pm = \sum_p e^{\pm ikp} S_p^\pm, \quad K^z = \sum_p S_p^z = S^z, \quad (15)$$

where k is the lattice momentum. In 1D $k = \frac{2\pi n}{M}$ with n being an integer restricted to $-\frac{M}{2} < n \leq \frac{M}{2}$. These three operators fulfill the $su(2)$ commutation algebra

$$[K_k^+, K_k^-] = 2K^z, \quad (16a)$$

$$[K^z, K_k^\pm] = \pm K_k^\pm \quad (16b)$$

Note that for momentum $k = 0$ the K - $su(2)$ algebra reduces to the spin $su(2)$ algebra.

This K - $su(2)$ algebra has been recently introduced in the context of quantum many-body scars in spin lattice systems [38, 39]. However, our goal here is to use it to construct a reference ansatz to study many-body correlations in spin lattice ground states.

The (non-normalized) multimodal extreme AGP state is a spin- $\frac{M}{2}$ multiplet,

$$|N_k\rangle = (K_k^+)^N |\Downarrow\rangle, \quad (17)$$

with $K^z = N - \frac{M}{2}$ and $K^2 = \frac{M}{2} (\frac{M}{2} + 1)$. In the special cases where $k = \frac{2\pi}{m}$ for $m = 1, 2, 3$, etc, the multimodal extreme AGP state is called unimodal, bimodal,

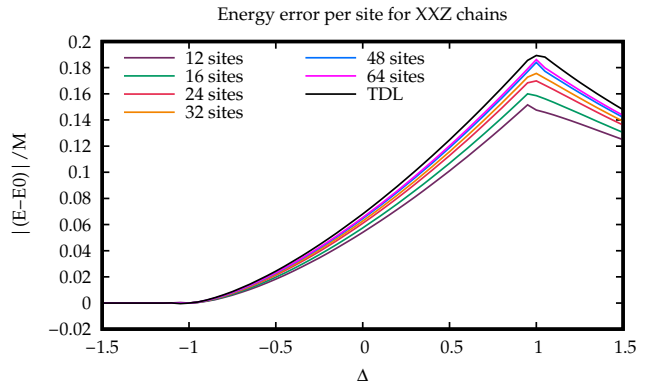


FIG. 3. Energy error per site for 1D XXZ chains with different lengths with open boundary conditions. The thermodynamic limit result is obtained by fitting the AGP energy result by the inverse of the lattice length. We notice that the per-site energy error grows as system size grows for $\Delta > -1$. It is also noticeable for $\Delta < -1$, the per-site energy error reduces as system size grows.

trimodal, etc, respectively, or m -modal in general. Note that in the m -modal extreme AGP, the η 's are just the m^{th} roots of unity. As with the bimodal extreme AGP, all multimodal extreme AGP states have the same average $\langle S^z \rangle$ on each site in the lattice.

We can now ask under which conditions the AGP states $|N_k\rangle$ are eigenstates of the XXZ Hamiltonian. As demonstrated in [35], it depends on the geometry of the lattice. For the 1D XXZ Hamiltonian with PBC, the condition is

$$\Delta = \cos(k) = \cos\left(\frac{2\pi n}{M}\right), \quad (18)$$

as shown in Appendix B. In these cases, we have

$$H_{\text{XXZ}} |N_k\rangle = \frac{M}{4} \Delta |N_k\rangle. \quad (19)$$

Moreover, the unimodal extreme AGP is the highest energy state at the Heisenberg point $\Delta = 1$, and the bimodal extreme AGP is the ground state for $\Delta = -1$. The result can also be extended to 1D lattice with OBC and bipartite 2D lattices, as shown in Appendix C. In the interval $-1 < \Delta = \cos\left(\frac{2\pi n}{M}\right) < 1$, the multimodal extreme AGPs are eigenstates of the Hamiltonian, known as scarred states, and they depict a nonthermal behavior [40, 41].

4. Approaching the Thermodynamic Limit

Figure 3 shows the energy error per site for the open boundary XXZ chain with different lengths in the $S^z = 0$ sector. The energy per site in the thermodynamic limit (TDL), e_0 , is extrapolated by fitting

$$\frac{E(M)}{M} = e_0 + e_1 \frac{1}{M} + e_2 \frac{1}{M^2} + \dots, \quad (20)$$

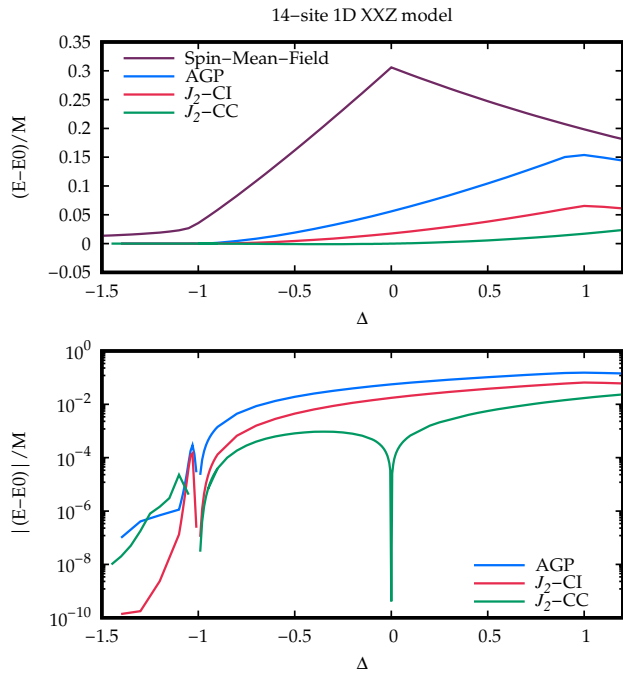


FIG. 4. Energy errors in the 14-site 1D XXZ model with open boundary conditions, in the $S^z = 0$ sector, in a linear scale (top panel) and logarithmic scale (bottom panel). We include sAGP as well as J_2 -CI and J_2 -CC results. We also include the standard spin mean-field result in the top panel in comparison with AGP.

where we truncate the expansion at second order $e_2 \frac{1}{M^2}$. We use the same extrapolation scheme for both the sAGP and the exact energies and display their differences in the TDL in Figure 3. We observe that for all lattice lengths, sAGP reaches its maximum error around $\Delta = 1$, and the value of Δ at which the error is the largest grows with the system size. The maximum sAGP error per site in the TDL is around 0.18. We can also see that sAGP is quite accurate in the ferromagnetic regime ($\Delta < -1$) for all system sizes; especially, as the system size grows, the per-site error reduces.

5. Incorporating Jastrow-Style Correlators

Although sAGP qualitatively captures the ferromagnetic, XY, and antiferromagnetic phases of the the 1D XXZ model, some correlation is still missing and needs to be recovered.

Correlating sAGP with the sAGP equivalent of the AGP killing operator [18],

$$K_{pq} = \eta_p^2 P_p^\dagger P_q + \eta_q^2 P_q^\dagger P_p + \frac{1}{2} \eta_p \eta_q (N_p N_q - N_p - N_q), \quad (21)$$

is not helpful here. This is because whenever $\eta_p^2 = \eta_q^2$, as in the case of a bimodal extreme AGP state, K_{pq} is

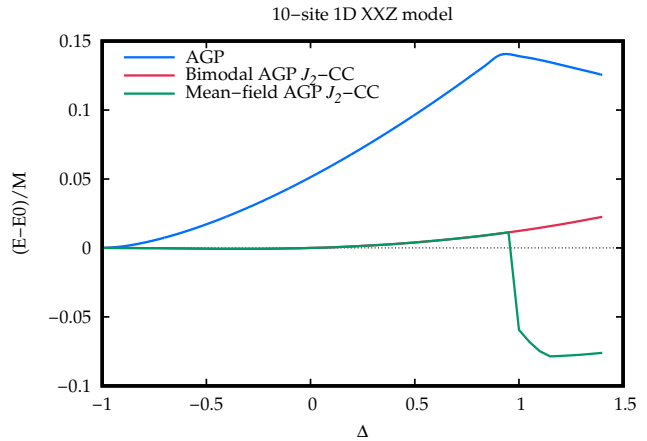


FIG. 5. Errors in the AGP and J_2 -CC energies based on the mean-field optimized AGP and the bimodal extreme AGP in the 10-site XXZ Heisenberg chain with open boundary conditions in the $S^z = 0$ sector.

Hermitian and K_{pq}^\dagger also kills the AGP.

Fortunately, we can use Hilbert space Jastrow correlators instead, which generate the same manifold as do the killing operators in the $\eta_p^2 \neq \eta_q^2$ case [19] because both ultimately correspond to a geminal replacement theory [30].

By Jastrow-style correlators, we mean operators of the form

$$J_2 = \frac{1}{4} \sum_{p < q} \alpha_{pq} N_p N_q \quad (22a)$$

$$\mapsto \sum_{p < q} \alpha_{pq} (2S_p^z - 1) (2S_q^z - 1). \quad (22b)$$

Since the lower-order Jastrow operator $J_1 = \sum \alpha_p N_p$ already lurks inside J_2 [31], we can define the J_2 operator for sAGP as

$$J_2 = \frac{1}{4} \sum_{p < q} \alpha_{pq} S_p^z S_q^z \quad (23)$$

and will use this definition hereafter.

The simplest way to correlate sAGP using these operators is by what we refer to as J_2 -CI, which writes

$$|J_2\text{-CI}\rangle = J_2 |s\text{AGP}\rangle, \quad (24)$$

where we generally use the mean-field optimized sAGP as a reference. We then evaluate the energy via an expectation value and minimize it with respect to the amplitudes α_{pq} .

Somewhat more sophisticated is J_2 -CC, where we use an exponential ansatz instead:

$$|J_2\text{-CC}\rangle = e^{J_2} |s\text{AGP}\rangle. \quad (25)$$

Although intractable in its variational incarnation, a similarity-transformed approach is quite feasible [31, 42].

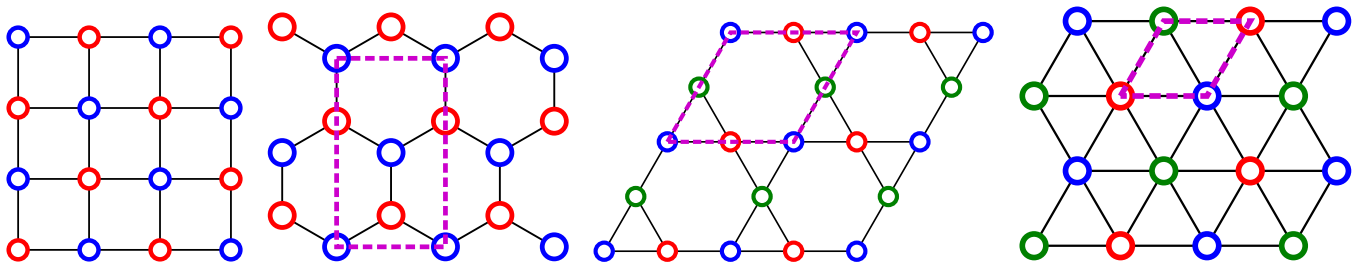


FIG. 6. Assorted 2D lattices. From left to right, these are the square lattice, the honeycomb lattice, the kagome lattice, and the triangular lattice. The purple dashed shape, wherever present, indicates the smallest rectangular cell for honeycomb lattice and the unit cell for kagome lattice and triangular lattice. The red, blue and green open circles indicate the different η values for the AGP ground state in the XXZ Hamiltonian, which is bimodal extreme for the square and honeycomb lattices, but trimodal extreme for the kagome and triangular lattices.

The energy and residual equations are

$$E_{J_2\text{-CC}} = \langle \text{sAGP} | \bar{H} | \text{sAGP} \rangle, \quad (26a)$$

$$0 = \langle \text{sAGP} | S_p^z S_q^z (\bar{H} - E_{J_2\text{-CC}}) | \text{sAGP} \rangle, \quad (26b)$$

where

$$\bar{H} = e^{-J_2} H e^{J_2}. \quad (27)$$

Although the commutator expansion of \bar{H} does not truncate, it can be analytically resummed to yield an expression in terms of exponentials of one-body operators J_1 , which act on one AGP state to produce another [31].

Figure 4 shows errors of $J_2\text{-CI}$ and $J_2\text{-CC}$ for the 14-site XXZ model with OBC. We see that $J_2\text{-CI}$ eliminates about half the error of AGP, while the improvement given by $J_2\text{-CC}$ is significantly larger, with an error an order of magnitude smaller than the error of AGP itself. This is particularly true when $J_2\text{-CC}$ is based on the bimodal extreme AGP everywhere, and not just where this is the lowest energy AGP (Figure 5). A particularly interesting feature is that $J_2\text{-CC}$ is exact at $\Delta = 0$. This is true in 1D but not in higher dimensions. In Appendix A, we prove this exactness for both open and periodic boundary conditions.

6. The Ferromagnetic XXZ Model

So far we have focused on the antiferromagnetic XXZ model, where $J = 1$. We now briefly discuss the ferromagnetic XXZ model, in which $J = -1$. Because of the Hamiltonian's overall sign change, the bimodal extreme AGP, which is the ground state for the antiferromagnetic XXZ model at $\Delta = -1$, becomes the highest energy eigenstate at this point for the ferromagnetic XXZ model. At the Heisenberg point $\Delta = 1$, however, the unimodal extreme AGP, where all $\eta_p = 1$, becomes the ground state for the ferromagnetic XXZ model for all S^z sectors with an energy of $E = -\frac{1}{4}M$ or $E = -\frac{1}{4}(M-1)$ for periodic boundary conditions and open boundary conditions, respectively.

B. The Two-Dimensional XXZ Model

We next test our methods on several XXZ 2D lattices including the square lattice, honeycomb lattice, triangular lattice, and kagome lattice (Fig. 6). In Appendix C, we show analytically that for both PBC and OBC with certain boundary shapes, the bimodal extreme AGP is the ground state of the square and honeycomb lattices at $\Delta = -1$, while the trimodal extreme AGP is the ground state of the triangular and kagome lattices at $\Delta = -0.5$. Particularly for the trimodal extreme AGP solution, the η values are

$$\eta_1 = 1, \quad \eta_2 = e^{i\frac{2}{3}\pi}, \quad \eta_3 = e^{i\frac{4}{3}\pi} \quad (28)$$

as defined in Sec. III A 3. The arrangements of the η values in different lattices are illustrated in Fig. 6. These analytical results are corroborated by numerical calculations as shown in Fig. 7. The ground states of the 2D XXZ models at these special Δ values have been reported in Ref. [34–36], though they are expressed in a form different from AGP.

While we do not wish to dwell on these various lattices in detail, we have a few things to point out.

First, as we can see in Fig. 8, sAGP is extreme over a range of Δ for all of the lattices. As with the 1D case, the sAGP ground state becomes non-extreme around $\Delta = 1$ for all of the 2D lattices considered here. It also becomes non-extreme for some negative Δ , but the crossover point is lattice-dependent. We notice that the crossover points for different lattices are correlated with the Δ values at which the extreme AGP is exact as discussed above.

Second, as shown in Fig. 9, $J_2\text{-CC}$ is no longer exact at $\Delta = 0$ for 2D lattices, as opposed to the 1D case. This is reminiscent of Jordan–Wigner transformed Hartree–Fock being exact at $\Delta = 0$ for the 1D spin models but not for their 2D counterparts [15, 43]. Although the results of $J_2\text{-CC}$ or $J_2\text{-CI}$ are not as good in 2D as they are in 1D, they still capture more than half of the correlation energy missing from the mean-field optimized sAGP methods.

Finally, we note that for the kagome lattice, we have been unable to find exact solutions of the $J_2\text{-CC}$ ampli-

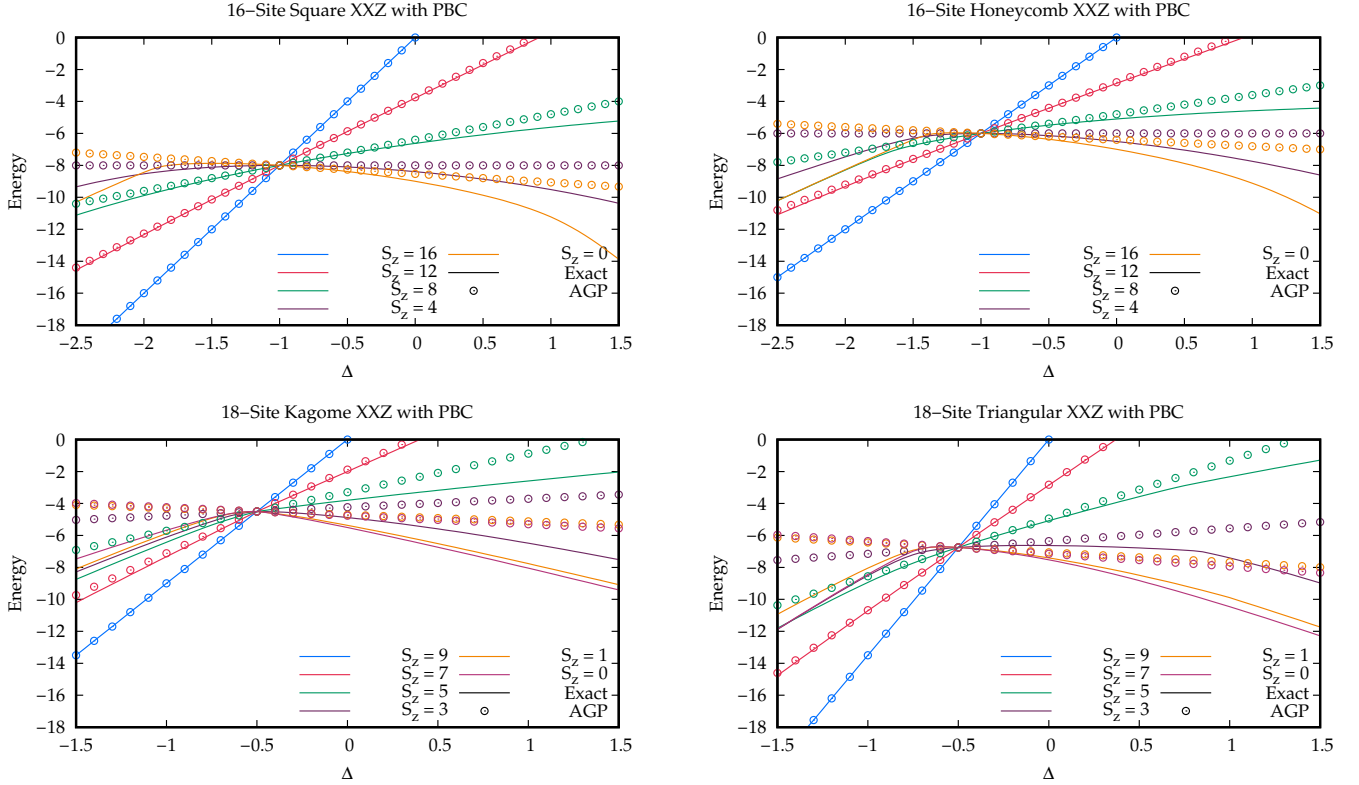


FIG. 7. Multimodal extreme AGP and exact energies of the XXZ Hamiltonian for different lattices and S^z sectors. The lines correspond to the exact energies and the circles to the multimodal extreme AGP results. Different colors correspond to different S^z sectors. Top left: square lattice. Top right: honeycomb lattice. Bottom left: kagome lattice. Bottom right: triangular lattice. All exact and AGP results have the same energy for all S^z sectors at $\Delta = -1$ (square or honeycomb lattice) or at $\Delta = -1/2$ (kagome or triangular lattice).

tude equations.

C. The $J_1 - J_2$ Model

We also test our sAGP-based methods on the 2D square $J_1 - J_2$ lattice with PBC:

$$H_{J_1 - J_2} = J_1 \sum_{\langle pq \rangle} (\vec{S}_p \cdot \vec{S}_q) + J_2 \sum_{\langle\langle pq \rangle\rangle} (\vec{S}_p \cdot \vec{S}_q), \quad (29)$$

where $\langle\langle pq \rangle\rangle$ denotes sites p and q being next-nearest neighbors. We take $J_1 = 1$, and vary J_2 . For $J_2 \ll 1$, the system is in a Néel order where all spins are antiparallel to their nearest neighbors. For $J_2 \gg 1$, the system is in a well-established striped order with spins parallel in the same column (or row) but antiparallel between columns (or rows). For $J_2 \approx 0.5$, however, the system is in a highly frustrated phase. The ground state is under debate and possible candidates include the plaquette valence-bond state [44], the stripe valence-bond state [45], or gapless spin liquid state [46].

We find that the optimized sAGP state for the $J_1 - J_2$ model shows a bimodal pattern over all interaction ranges like the case of XXZ between $-1 < \Delta < 1$ (Figure

11). For $J_2 < 1/2$, the η values show a Néel pattern, while for $J_2 > 1/2$, η values exhibit a striped pattern. The two patterns are degenerate at $J_2 = 1/2$. As is shown in Table I, for small system sizes, the optimized sAGP is bimodal but non-extreme ($|\eta_1| \neq |\eta_2|$), though the bimodal extreme state ($\eta_1 = 1, \eta_2 = -1$) is still a local minimum. For large system size, the bimodal extreme AGP becomes lower in energy than the non-extreme AGP.

TABLE I. Energy of the $J_1 - J_2$ model at $J_2 = 1/2$ for different system sizes. We see the energy is only dependent on the system size. For small system sizes, the optimized sAGP is bimodal but non-extreme while for large system size, the bimodal extreme AGP becomes lower in energy than the non-extreme AGP.

| System Size | Extreme | Non-extreme | Energy Difference |
|----------------|----------|-------------|-------------------|
| 4×4 | -5.0667 | -5.2672 | 0.2005 |
| 4×8 | -9.0323 | -9.2417 | 0.2094 |
| 4×16 | -17.0245 | -17.2296 | 0.2050 |
| 8×8 | -17.0245 | -17.2296 | 0.2050 |
| 8×12 | -25.1109 | -25.2256 | 0.1146 |
| 12×12 | -37.4387 | -37.2230 | -0.2157 |
| 16×16 | -66.4843 | -65.2206 | -1.2637 |

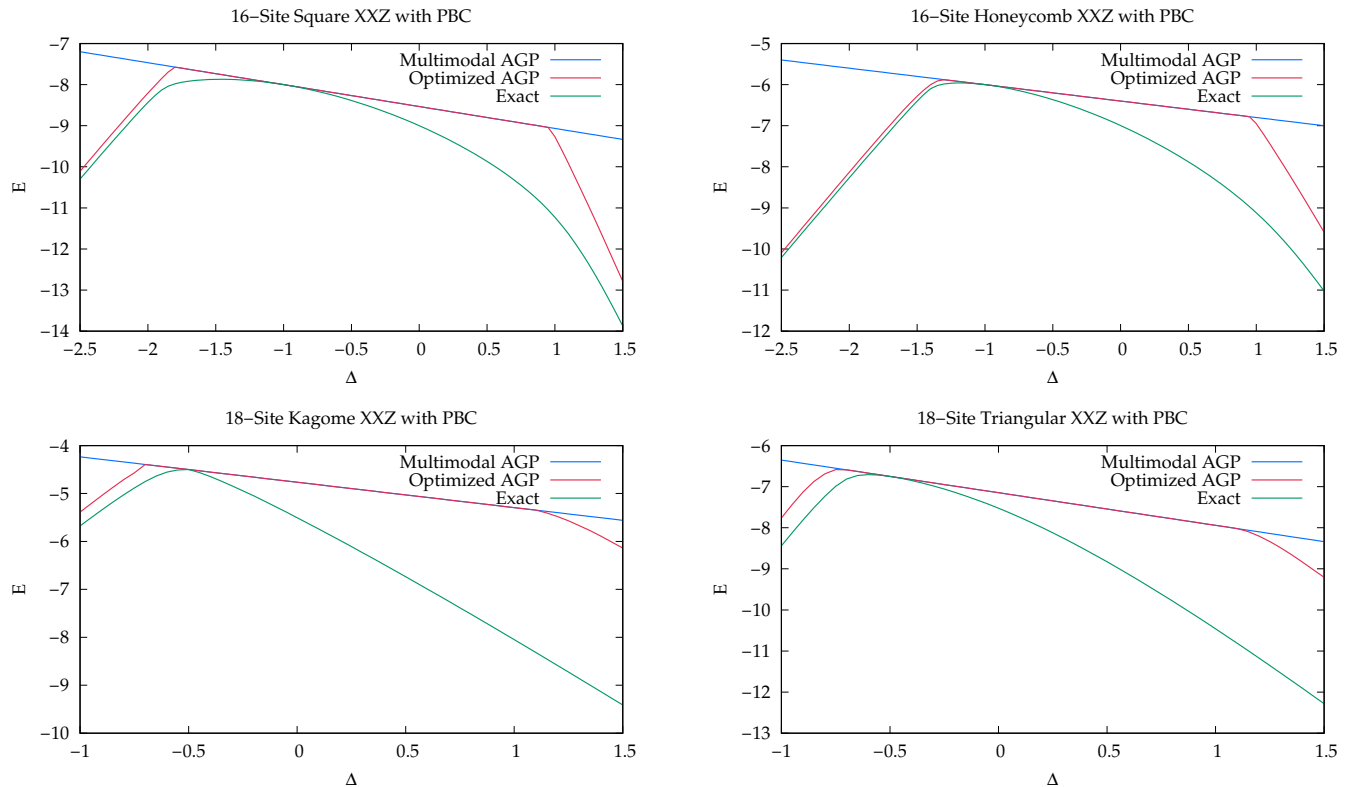


FIG. 8. Exact energies and those of the multimodal extreme AGP and mean-field optimized AGP for the XXZ Hamiltonian with $S^z = 0$. Top left: 16-site square lattice. Top right: 16-site honeycomb lattice. Bottom left: 18-site kagome lattice. Bottom right: 18-site triangular lattice.

Figure 10 shows the energies of the bimodal extreme AGP and its correlated methods for the 4×4 $J_1 - J_2$ model. The two branches of the sAGP curve correspond to the two bimodal extreme patterns (Néel versus striped).

The J_2 -CC (Eqn. (25)) energy exhibits a discontinuity at $J_2 = 1/2$ because of the two branches of the reference sAGP. Moreover, for $0.43 < J_2 < 0.5$ (the tail of the left branch in Fig. 10), the J_2 -CC residual equations fail to converge, so rather than solving them exactly, we minimize the norm of the residuals instead.

In order to remove the discontinuity and produce well-behaved curves, we consider a reference state that is a linear combination of the relevant sAGPs (LC-AGP). This is simply an sAGP-based non-orthogonal CI [27]. We find that at least 7 bimodal extreme AGPs are needed if we want to approximate the exact ground state (with additional J_2 -CI-type correlation; vide infra). They include the bimodal extreme AGP with the Néel pattern and those with the column-wise and row-wise striped patterns, as well as four additional intermediate bimodal extreme AGP states shown in Fig. 12. These intermediate bimodal extreme AGPs exhibit a pattern between Néel and striped where each site has only one nearest neighbor that shares its η value.

We see that the LC-AGP is well-behaved near $J_2 = 1/2$

but offers little quantitative improvement over a single sAGP elsewhere. In practice, this means that J_2 -CC or J_2 -CI based on this LC-AGP looks little different from the corresponding methods based on the mean-field optimized sAGP, except for $J_2 \approx 1/2$. Thus, we consider linear combinations of J_2 -CI states as well, shown in Fig. 10 as AGP-LC- J_2 -CI. This LC- J_2 -CI is roughly parallel to the exact result, and is comparable to J_2 -CC, but is correctly smooth everywhere.

IV. CONCLUSIONS

In this article, we have studied spin AGP and several spin AGP based correlation methods for the 1D and 2D XXZ models, and the 2D $J_1 - J_2$ model. With our $\mathcal{O}(M^3)$ implementation of mean-field optimized AGP, we find that optimized spin AGP can capture the phase transitions of the XXZ Heisenberg chain and 2D lattices. Furthermore, we show that the optimized AGP states turn out to be multimodal extreme for the $J_1 - J_2$ model and the XY phase of the XXZ model, reflecting the translational symmetry of these states. The fact that all η 's have the same absolute value makes the calculation of correlation methods based on sAGP even easier. These facts suggest that spin AGP should be a good reference

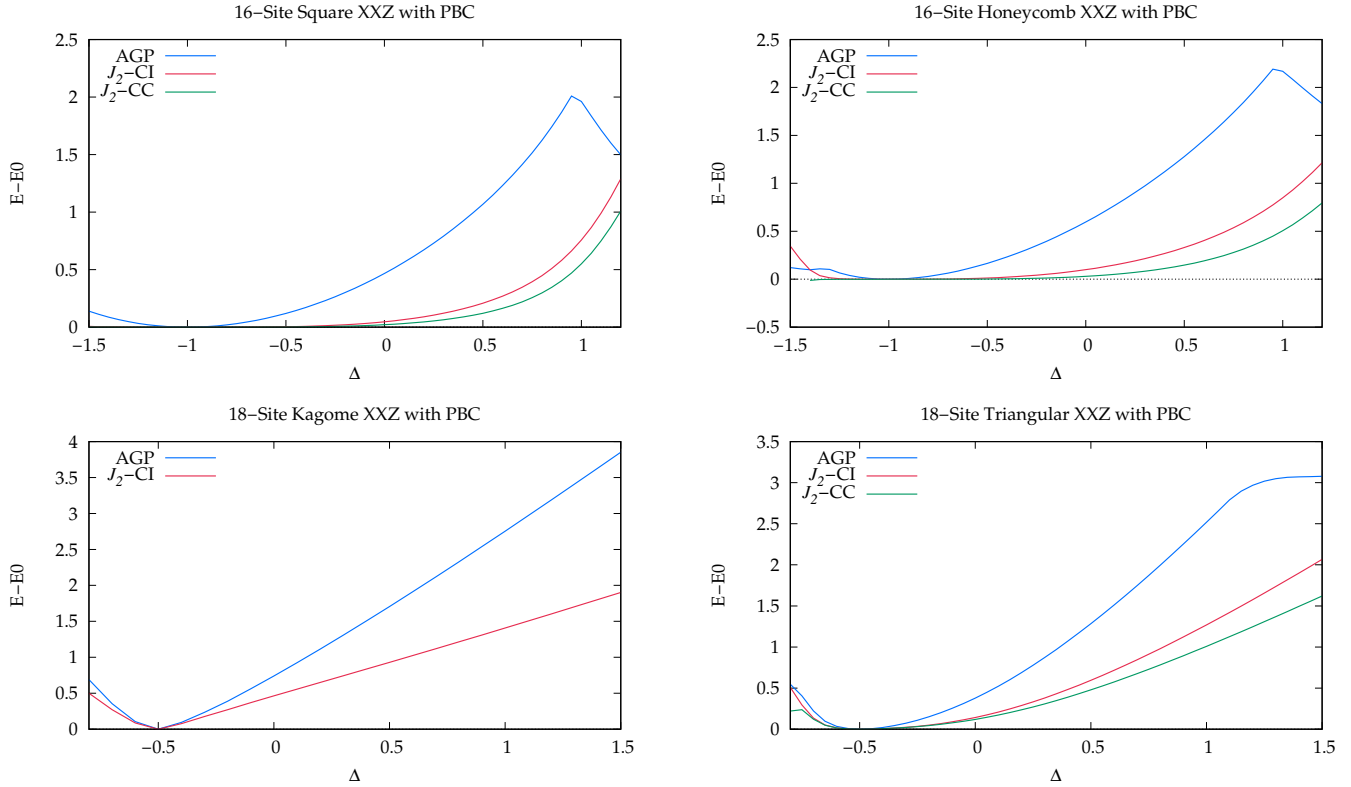


FIG. 9. Energy errors for the mean-field optimized AGP and for J_2 -CI and J_2 -CC based on the multimodal extreme AGP, in various XXZ lattices with $S^z = 0$. Top left: 16-site square lattice. Top right: 16-site honeycomb lattice. Bottom left: 18-site kagome lattice. Bottom right: 18-site triangular lattice. Note that J_2 -CC does not converge for the kagome lattice and has been omitted from the plot.

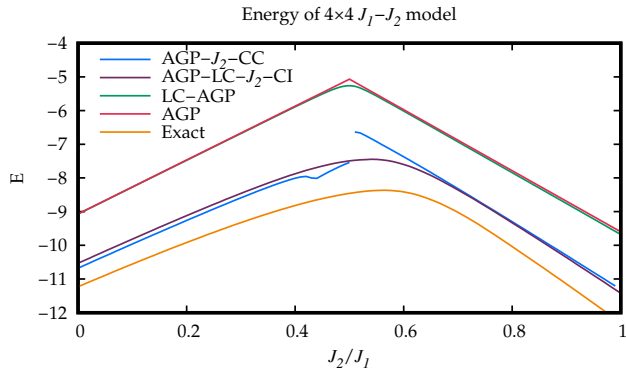


FIG. 10. Energy error for the 4×4 $J_1 - J_2$ model with PBC. The exact energy is calculated with exact diagonalization. AGP is the bimodal extreme AGP. LC-AGP is a linear combination of 7 bimodal extreme AGPs. AGP- J_2 -CC and AGP-LC- J_2 -CI are correlated methods based on AGP and LC-AGP, respectively.

state for these spin systems.

Though correlation methods based on killing operators [18] are not feasible for spin AGP, we show that Jastrow operators can serve as good correlators for spin systems.

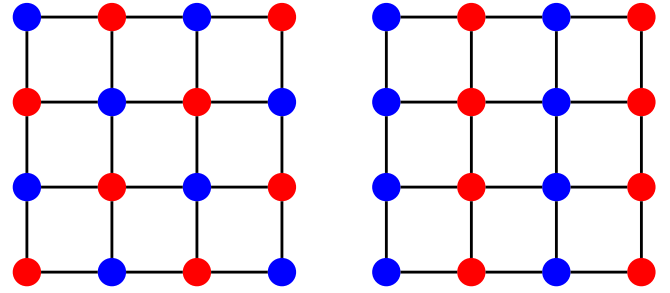


FIG. 11. The AGP η pattern for the 4×4 $J_1 - J_2$ model with PBC. All sites with the same color have the same η value. The left figure corresponds to $J_2 < 0.5$, and the right $J_2 > 0.5$

Both J_2 -CI and J_2 -CC yield a significant improvement over mean-field optimized AGP with reasonable computational cost; J_2 -CC behaves especially well in the XY phase $-1 < \Delta \lesssim 1$ for the XXZ chain, and is exact at $\Delta = 0$ in 1D.

We have also shown that for the 2D $J_1 - J_2$ model, there are multiple important bimodal extreme AGP states. The LC-AGP approach uses a linear combination of these important AGP states and makes the transition between the Néel pattern and striped pattern smooth.

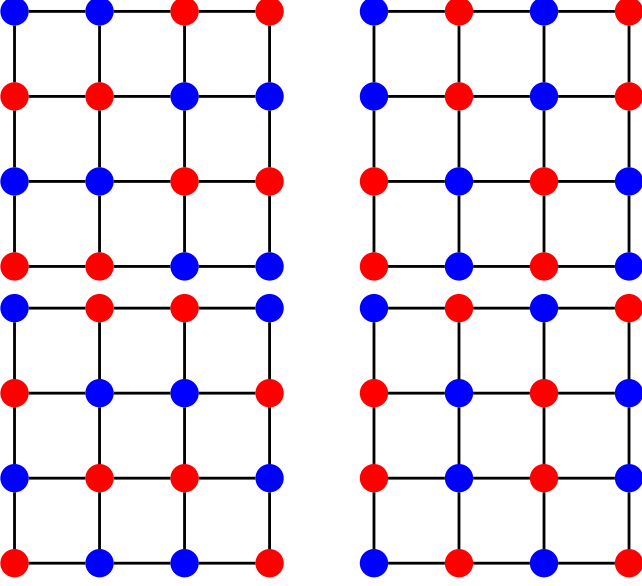


FIG. 12. The four intermediate bimodal extreme AGP states necessary for LC-AGP and LC- J_2 -CI for the $4 \times J_1 - J_2$ model with PBC.

The LC- J_2 -CI energy result on $J_1 - J_2$ model is almost parallel to the exact one.

Thus far, we have considered only energies. The behavior of our techniques for correlation functions and other properties will be reported in future work.

ACKNOWLEDGMENTS

This work was supported by the U.S. National Science Foundation under Grant No. CHE-2153820. G.E.S. is a Welch Foundation Chair (Grant No. C-0036). J.D. acknowledges financial support from Project No. PGC2018-094180-B-I00 (MCIU/AEI/FEDER, EU).

Appendix A: Exactness of J_2 -CC for 1D XXZ at $\Delta = 0$

A general wave function for an M -site 1D spin- $\frac{1}{2}$ system can be written as

$$|\psi\rangle = \sum_{1 \leq p_1 < \dots < p_N \leq M} \psi(p_1, \dots, p_N) S_{p_1}^\dagger \dots S_{p_N}^\dagger \quad (\text{A1})$$

where $\psi(p_1, \dots, p_N)$ is the amplitude for the N \uparrow -spins at sites p_1, \dots, p_N .

Exact eigenvalues and eigenstates of the 1D XXZ model with periodic boundary conditions can be found by the Bethe ansatz, where the ground state amplitude

can be written as

$$\psi(p_1, \dots, p_N) = \sum_{\sigma \in S_N} A(\sigma) \exp\left(i \sum_{j=1}^N k_{\sigma(j)} p_j\right). \quad (\text{A2})$$

The summation runs over all $N!$ permutations of $1, \dots, N$. The amplitudes A relate to the scattering matrix S through

$$A(\nu) = S(k_i, k_j) A(\sigma), \quad (\text{A3})$$

where the permutation ν is related to the permutation σ by swapping i with j , and

$$S(k_i, k_j) = -\frac{e^{i(k_i+k_j)} - 2\Delta e^{ik_j} + 1}{e^{i(k_i+k_j)} - 2\Delta e^{ik_i} + 1}. \quad (\text{A4})$$

For the case $\Delta = 0$, $S(k_i, k_j) = -1$, and we can choose $A(\sigma) = (-1)^{\text{sgn}(\sigma)}$. The parameters k_1, \dots, k_n in Eqn. (A2) can be solved by the Bethe ansatz equations:

$$e^{ik_i M} = \prod_{j \neq i} S(k_i, k_j). \quad (\text{A5})$$

For even N , the equations reduce to

$$e^{ik_i M} = -1 \quad (\text{A6})$$

and k_i are

$$k_i - \pi = \{\pm\pi/M, \pm 3\pi/M, \pm 5\pi/M \dots\}. \quad (\text{A7})$$

The amplitude $\psi(p_1, \dots, p_N)$ can thus be written as

$$\psi(p_1, \dots, p_N) = \det(C) \quad (\text{A8})$$

where the matrix C is defined by $C_{ij} = e^{ik_i p_j}$ and can be recognized as a Vandermonde matrix. Therefore,

$$\det(C) = \prod_{1 \leq i < j \leq N} \sin\left(\frac{\pi}{M}(p_j - p_i)\right) \prod_{l=1}^N e^{i\pi p_l}. \quad (\text{A9})$$

According to Eqns. (A8) and (A9), the wave function can be written as J_2 -CC on the bimodal extreme AGP:

$$|\psi\rangle = e^{J_2} |\text{AGP}\rangle \quad (\text{A10})$$

with $\eta_p = e^{i\pi p}$, and J_2 coefficients satisfying

$$\alpha_{pq} = \ln\left(\sin\left(\frac{\pi}{M}(q-p)\right)\right) \quad (\text{A11})$$

for all $1 \leq p < q \leq M$.

For open boundary conditions, the derivation is essentially the same, and the ground state amplitude can still be written as a determinant, but now

$$\det(C) = \prod_{1 \leq i < j \leq N} 2 \left(\cos \left(\frac{\pi p_j}{M+1} \right) - \cos \left(\frac{\pi p_i}{M+1} \right) \right) \prod_{l=1}^N \sin \left(\frac{\pi p_l}{M+1} \right). \quad (\text{A12})$$

This can be written as J_2 -CC on AGP with coefficients

$$\eta_p = \sin \left(\frac{\pi p}{M+1} \right), \quad (\text{A13a})$$

$$\alpha_{pq} = \ln \left(2 \left(\cos \left(\frac{\pi q}{M+1} \right) - \cos \left(\frac{\pi p}{M+1} \right) \right) \right). \quad (\text{A13b})$$

This η values are not extreme. However, since the J_2 operator contains J_1 , and J_1 transforms the η values [31], this means J_2 -CC on bimodal extreme AGP is also exact.

Appendix B: Multimodal Extreme AGP as the Eigenstate of 1D XXZ with PBC

We want to show the multimodal extreme AGP Eqn. (17) generated by the K_k^+ operator Eqn. (15) is an eigenstate of the 1D XXZ Hamiltonian with PBC when $\Delta = \cos k$.

First we compute the commutators of H_{XXZ} with K_k^+ . Using

$$\left[\sum_{p=1}^M \frac{1}{2} (S_p^+ S_{p+1}^- + S_p^- S_{p+1}^+), K_k^+ \right] = - \sum_{p=1}^M (e^{ik} e^{ikp} S_p^+ S_{p+1}^z + e^{ikp} S_{p+1}^+ S_p^z), \quad (\text{B1a})$$

$$\left[\sum_{p=1}^M S_p^z S_{p+1}^z, K_k^+ \right] = \sum_{p=1}^M (e^{ik} e^{ikp} S_{p+1}^+ S_p^z + e^{ikp} S_p^+ S_{p+1}^z), \quad (\text{B1b})$$

we obtain

$$[H_{\text{XXZ}}, K_k^+] = (\Delta - e^{ik}) \sum_{p=1}^M e^{ikp} S_p^+ S_{p+1}^z + (\Delta e^{ik} - 1) \sum_{p=1}^M e^{ikp} S_{p+1}^+ S_p^z, \quad (\text{B2})$$

$$[[H_{\text{XXZ}}, K_k^+], K_k^+] = (\Delta - e^{ik}) e^{ik} \sum_{p=1}^M e^{2ikp} S_p^+ S_{p+1}^+ + (\Delta e^{ik} - 1) \sum_{p=1}^M e^{2ikp} S_{p+1}^+ S_p^+ \quad (\text{B3a})$$

$$= (2\Delta e^{ik} - e^{2ik} - 1) \sum_{p=1}^M e^{2ikp} S_p^+ S_{p+1}^+. \quad (\text{B3b})$$

We also have

$$[H_{\text{XXZ}}, K_k^+] |\Downarrow\rangle = -\frac{1}{2} \left((\Delta - e^{ik}) \sum_{p=1}^M e^{ikp} S_p^+ + (\Delta e^{ik} - 1) \sum_{p=1}^M e^{ikp} S_{p+1}^+ \right) |\Downarrow\rangle \quad (\text{B4a})$$

$$= -\frac{1}{2} \left((\Delta - e^{ik}) \sum_{p=1}^M e^{ikp} S_p^+ + (\Delta e^{ik} - 1) e^{-ik} \sum_{p=1}^M e^{ik(p+1)} S_{p+1}^+ \right) |\Downarrow\rangle \quad (\text{B4b})$$

$$= -\frac{1}{2} (2\Delta - e^{ik} - e^{-ik}) \sum_{p=1}^M e^{ikp} S_p^+ |\Downarrow\rangle. \quad (\text{B4c})$$

When $\Delta = \cos k$, we have $(2\Delta - e^{ik} - e^{-ik}) = 0$, thus

$$[[H_{\text{XXZ}}, K_k^+], K_k^+] = 0, \quad (\text{B5a})$$

$$[H_{\text{XXZ}}, K_k^+] |\Downarrow\rangle = 0. \quad (\text{B5b})$$

Then we can calculate $H_{\text{XXZ}} |N_k\rangle$:

$$H_{\text{XXZ}} |N_k\rangle = H_{\text{XXZ}} (K_k^+)^N |\Downarrow\rangle \quad (\text{B6a})$$

$$= N(K_k^+)^{N-1} [H_{\text{XXZ}}, K_k^+] |\Downarrow\rangle + \frac{N(N-1)}{2} (K_k^+)^{N-2} [[H_{\text{XXZ}}, K_k^+], K_k^+] |\Downarrow\rangle + (K_k^+)^N H_{\text{XXZ}} |\Downarrow\rangle \quad (\text{B6b})$$

$$= \frac{M}{4} \Delta (K_k^+)^N |\Downarrow\rangle \quad (\text{B6c})$$

$$= \frac{M}{4} \Delta |N_k\rangle. \quad (\text{B6d})$$

We see that the multimodal extreme AGP $|N_k\rangle$ becomes an eigenstate of the Hamiltonian H_{XXZ} in 1D, with PBC.

Appendix C: Multimodal Extreme AGP as the Ground State of Colorable XXZ for Certain Δ

The proof in the previous appendix relies on properties of the K_k^+ operator to show that extreme multimodal AGP is an eigenstate of the 1D XXZ Hamiltonian with PBC. In fact, as we have noted in the text, multimodal extreme AGP is the exact ground state at certain values of Δ even in multiple dimensions. Here, we wish to sketch a proof of this claim. Fuller details can be found in the supporting information.

1. Bimodal Extreme AGP for Bipartite Lattices

Bimodal extreme AGP is the ground state for the 1D XXZ chain and 2D square and honeycomb lattices at $\Delta = -1$. In fact it is the ground state at this Δ for any lattice so long as the lattice can be colored with only 2 colors so that each pair of neighboring sites has different color (i.e. for any bipartite lattice).

Say p, q are neighboring sites. Let

$$H_{pq} = \frac{(S_p^+ S_q^- + S_p^- S_q^+)}{2} + \Delta S_p^z S_q^z. \quad (\text{C1})$$

The XXZ Hamiltonian can then be written as

$$H_{\text{XXZ}} = \sum_{\langle pq \rangle} H_{pq}. \quad (\text{C2})$$

We will show that bimodal extreme AGP is the ground state not only of the whole Hamiltonian H_{XXZ} , but also for each bond H_{pq} .

The spin AGP is

$$|\text{sAGP}\rangle = \frac{1}{N!} \left(\sum_{p=1}^M \eta_p S_p^+ \right) |\Downarrow\rangle \quad (\text{C3a})$$

$$= \sum_{1 \leq p_1 < \dots < p_N \leq M} \eta_{p_1} \dots \eta_{p_N} S_{p_1}^+ \dots S_{p_N}^+ |\Downarrow\rangle. \quad (\text{C3b})$$

For a given pair of nearest neighbors p and q , AGP can be written as

$$\begin{aligned} |\text{sAGP}\rangle & \quad (\text{C4}) \\ &= \sum_{\sim} c_{uu} \eta_p \eta_q |\sim \uparrow_p \uparrow_q \sim\rangle + \sum_{\sim} c_{dd} |\sim \downarrow_p \downarrow_q \sim\rangle \\ &+ \sum_{\sim} c_{ud} \eta_p |\sim \uparrow_p \downarrow_q \sim\rangle + \sum_{\sim} c_{du} \eta_q |\sim \downarrow_p \uparrow_q \sim\rangle. \end{aligned}$$

Here, \sim represents all possible situations of the sites other than p and q . c_{uu} , c_{du} , c_{ud} , c_{dd} are the products of the η s on each site with \uparrow spin in \sim .

The two summations for $|\sim \downarrow_p \downarrow_q \sim\rangle$ and $|\sim \uparrow_p \downarrow_q \sim\rangle$ are the same, as there are $M-2$ other sites, $N-1$ of which have \uparrow spin. For the same reason $c_{ud} = c_{du}$, so

$$\begin{aligned} |\text{sAGP}\rangle &= \sum_{\sim} c_{uu} \eta_p \eta_q |\sim \uparrow_p \uparrow_q \sim\rangle + \sum_{\sim} c_{dd} |\sim \downarrow_p \downarrow_q \sim\rangle \\ &+ \sum_{\sim} c_{ud} (\eta_p |\sim \uparrow_p \downarrow_q \sim\rangle + \eta_q |\sim \downarrow_p \uparrow_q \sim\rangle). \quad (\text{C5}) \end{aligned}$$

For bimodal extreme AGP, $\eta_p = -\eta_q$, so that

$$\begin{aligned} |\text{sAGP}\rangle &= - \sum_{\sim} c_{uu} |\sim \uparrow_p \uparrow_q \sim\rangle + \sum_{\sim} c_{dd} |\sim \downarrow_p \downarrow_q \sim\rangle \\ &+ \sum_{\sim} c_{ud} \eta_p (|\sim \uparrow_p \downarrow_q \sim\rangle - |\sim \downarrow_p \uparrow_q \sim\rangle). \quad (\text{C6}) \end{aligned}$$

Now note that

$$H_{pq} |\sim \uparrow_p \uparrow_q \sim\rangle = \Delta S_p^z S_q^z |\sim \uparrow_p \uparrow_q \sim\rangle = \frac{\Delta}{4} |\sim \uparrow_p \uparrow_q \sim\rangle \quad (\text{C7})$$

$$H_{pq} |\sim \downarrow_p \downarrow_q \sim\rangle = \Delta S_p^z S_q^z |\sim \downarrow_p \downarrow_q \sim\rangle = \frac{\Delta}{4} |\sim \downarrow_p \downarrow_q \sim\rangle \quad (\text{C8})$$

$$H_{pq} (|\sim \uparrow_p \downarrow_q \sim\rangle - |\sim \downarrow_p \uparrow_q \sim\rangle) \quad (\text{C10a})$$

$$= \left(\frac{S_p^+ S_q^- + S_p^- S_q^+}{2} + \Delta S_p^z S_q^z \right) (|\sim \uparrow_p \downarrow_q \sim\rangle - |\sim \downarrow_p \uparrow_q \sim\rangle) \quad (\text{C10b})$$

$$= \left(-\frac{1}{2} - \frac{1}{4} \Delta \right) (|\sim \uparrow_p \downarrow_q \sim\rangle - |\sim \downarrow_p \uparrow_q \sim\rangle). \quad (\text{C10c})$$

When $\Delta = -1$, we obtain

$$H_{pq} |\text{sAGP}\rangle = -\frac{1}{4} |\text{sAGP}\rangle. \quad (\text{C11})$$

This shows that the bimodal extreme AGP is an eigenstate of every bond H_{pq} in the lattice at $\Delta = -1$.

Now we will show it is the ground state at this Δ . Recall the Hamiltonian of the single bond, given in Eqn (C1). For any states of the entire lattice, only the spin configurations at site p and q have an influence on the single bond, so we can safely project the state to the subspace that only contains these 2 sites and diagonalize the Hamiltonian of the bond in this subspace. The eigenvalues are $-\frac{1}{4}, -\frac{1}{4}, -\frac{1}{4}, \frac{1}{4}$. The bimodal extreme AGP energy of $-\frac{1}{4}$ means that it is a ground state for this single bond. Thus bimodal extreme AGP is a ground state for all bonds in the lattice at $\Delta = -1$. This means it is also a ground state of the entire Hamiltonian, and

$$H_{\text{XXZ}} |\text{sAGP}\rangle = -\frac{\text{Number of bonds}}{4} |\text{sAGP}\rangle. \quad (\text{C12})$$

Note that this result relies only on the form of the Hamiltonian and on the lattice being bipartite. In particular,

$$\begin{aligned} |\text{sAGP}\rangle &= \sum_{\sim} c_{uuu} \eta_p \eta_q \eta_r |\sim \uparrow_p \uparrow_q \uparrow_r \sim\rangle \\ &+ \sum_{\sim} c_{uud} (\eta_p \eta_q |\sim \uparrow_p \uparrow_q \downarrow_r \sim\rangle + \eta_p \eta_r |\sim \uparrow_p \downarrow_q \uparrow_r \sim\rangle + \eta_r \eta_q |\sim \downarrow_p \uparrow_q \uparrow_r \sim\rangle) \\ &+ \sum_{\sim} c_{udd} (\eta_p |\sim \uparrow_p \downarrow_q \downarrow_r \sim\rangle + \eta_q |\sim \downarrow_p \uparrow_q \downarrow_r \sim\rangle + \eta_r |\sim \downarrow_p \downarrow_q \uparrow_r \sim\rangle) \\ &+ \sum_{\sim} c_{ddd} |\sim \downarrow_p \downarrow_q \downarrow_r \sim\rangle. \end{aligned} \quad (\text{C14})$$

Following a similar procedure as we have outlined for the two-colorable case, it can be shown that

$$H_{\Delta} |\text{sAGP}\rangle = -\frac{3}{8} |\text{sAGP}\rangle. \quad (\text{C15})$$

Thus the trimodal extreme AGP is the ground of state

it is true for any number of dimensions, for any boundary conditions, and for any (integer) S^z sector.

2. Trimodal Extreme AGP for Tripartite Lattices

The kagome and triangular lattices cannot be colored with only 2 colors due to the triangular shape (Fig.6). These lattices are three-colorable (i.e. tripartite). We will show trimodal extreme AGP is an eigenstate of the triangular shapes in the three-colorable lattices.

Say p, q, r are 3 sites that form a triangle. In trimodal extreme AGP, η_p, η_q, η_r are correspondingly $1, e^{\pm \frac{2i\pi}{3}}$. Let

$$H_{\Delta} = H_{pq} + H_{qr} + H_{rp}. \quad (\text{C13})$$

The trimodal extreme AGP, when focusing on these three sites, is

of a triangle that contains the 3 different η . In periodic boundary conditions, both kagome and triangular lattices are composed purely of such triangles, and trimodal extreme AGP is the exact ground state at $\Delta = -0.5$. For open boundary conditions, trimodal extreme AGP is the exact ground state at $\Delta = -0.5$ only when the lattice breaks none of these triangles.

of a triangle that contains the 3 different η . In periodic boundary conditions, both kagome and triangular lattices are composed purely of such triangles, and trimodal extreme AGP is the exact ground state at $\Delta = -0.5$. For open boundary conditions, trimodal extreme AGP is the exact ground state at $\Delta = -0.5$ only when the lattice breaks none of these triangles.

-
- [1] U. Schollwöck, J. Richter, D. J. Farnell, and R. F. Bishop, *Quantum magnetism*, Vol. 645 (Springer, 2008).
 - [2] Z.-H. Cui, H. Zhai, X. Zhang, and G. K.-L. Chan, *Science* **377**, 1192 (2022).
 - [3] L. Noodleman, C. Peng, D. Case, and J.-M. Mouesca, *Coord. Chem. Rev.* **144**, 199 (1995).
 - [4] E. J. Davis, B. Ye, F. Machado, S. A. Meynell, W. Wu, T. Mittiga, W. Schenken, M. Joos, B. Kobrin, Y. Lyu, *et al.*, arXiv preprint arXiv:2103.12742 (2021).
 - [5] J. J. García-Ripoll, M. A. Martin-Delgado, and J. I. Cirac, *Phys. Rev. Lett.* **93**, 250405 (2004).
 - [6] C. Broholm, R. J. Cava, S. A. Kivelson, D. G. Nocera, M. R. Norman, and T. Senthil, *Science* **367**, eaay0668 (2020).
 - [7] A. Kitaev, *Ann. Phys.* **321**, 2 (2006).
 - [8] S. Yan, D. A. Huse, and S. R. White, *Science* **332**, 1173 (2011).
 - [9] S. R. White and A. L. Chernyshev, *Phys. Rev. Lett.* **99**, 127004 (2007).
 - [10] D. Sellmann, X.-F. Zhang, and S. Eggert, *Phys. Rev. B* **91**, 081104(R) (2015).
 - [11] Z. Zhu and S. R. White, *Phys. Rev. B* **92**, 041105(R) (2015).
 - [12] W.-Y. Liu, S.-S. Gong, Y.-B. Li, D. Poilblanc, W.-Q.

- Chen, and Z.-C. Gu, *Sci. Bull.* **67**, 1034 (2022).
- [13] R. F. Bishop, J. B. Parkinson, and Y. Xian, *Phys. Rev. B* **46**, 880 (1992).
- [14] R. F. Bishop, D. J. Farnell, and J. B. Parkinson, *J. Phys.: Condens. Matter* **8**, 11153 (1996).
- [15] T. M. Henderson, G. P. Chen, and G. E. Scuseria, *J. Chem. Phys.* **157**, 194114 (2022).
- [16] A. J. Coleman, *J. Math. Phys.* **6**, 1425 (1965).
- [17] P. Ring and P. Schuck, *The nuclear many-body problem* (Springer Science & Business Media, 2004).
- [18] T. M. Henderson and G. E. Scuseria, *J. Chem. Phys.* **151**, 051101 (2019).
- [19] T. M. Henderson and G. E. Scuseria, *J. Chem. Phys.* **153**, 084111 (2020).
- [20] J. Bardeen, L. N. Cooper, and J. R. Schrieffer, *Phys. Rev.* **108**, 1175 (1957).
- [21] C. N. Yang, *Rev. Mod. Phys.* **34**, 694 (1962).
- [22] P. W. Anderson, *Mater. Res. Bull.* **8**, 153 (1973).
- [23] P. W. Anderson, G. Baskaran, Z. Zou, and T. Hsu, *Phys. Rev. Lett.* **58**, 2790 (1987).
- [24] L.-K. Hua, *Am. J. Math.* **66**, 470 (1944).
- [25] G. E. Scuseria, C. A. Jiménez-Hoyos, T. M. Henderson, K. Samanta, and J. K. Ellis, *J. Chem. Phys.* **135**, 124108 (2011).
- [26] A. Khamoshi, T. M. Henderson, and G. E. Scuseria, *J. Chem. Phys.* **151**, 184103 (2019).
- [27] R. Dutta, G. P. Chen, T. M. Henderson, and G. E. Scuseria, *J. Chem. Phys.* **154**, 114112 (2021).
- [28] P. W. Anderson, *Phys. Rev.* **112**, 1900 (1958).
- [29] L. Bytautas, T. M. Henderson, C. A. Jiménez-Hoyos, J. K. Ellis, and G. E. Scuseria, *J. Chem. Phys.* **135**, 044119 (2011).
- [30] R. Dutta, T. M. Henderson, and G. E. Scuseria, *J. Chem. Theory Comput.* **16**, 6358 (2020).
- [31] A. Khamoshi, G. P. Chen, T. M. Henderson, and G. E. Scuseria, *J. Chem. Phys.* **154**, 074113 (2021).
- [32] A. Khamoshi, F. A. Evangelista, and G. E. Scuseria, *Quantum Sci. Technol.* **6**, 014004 (2020).
- [33] A. Khamoshi, G. P. Chen, F. A. Evangelista, and G. E. Scuseria, *Quantum Sci. Technol.* **8**, 015006 (2023).
- [34] H. J. Changlani, D. Kochkov, K. Kumar, B. K. Clark, and E. Fradkin, *Phys. Rev. Lett.* **120**, 117202 (2018).
- [35] S. Pal, P. Sharma, H. J. Changlani, and S. Pujari, *Phys. Rev. B* **103**, 144414 (2021).
- [36] E. Chertkov and B. K. Clark, *Phys. Rev. B* **104**, 104410 (2021).
- [37] C. N. Yang and C. P. Yang, *Phys. Rev.* **150**, 321 (1966).
- [38] N. O’Dea, F. Burnell, A. Chandran, and V. Khemani, *Phys. Rev. Res.* **2**, 043305 (2020).
- [39] J. Ren, C. Liang, and C. Fang, *Phys. Rev. Res.* **4**, 013155 (2022).
- [40] N. Regnault, S. Moudgalya, and B. A. Bernevig, *Rep. Prog. Phys.* (2022).
- [41] R. Melendrez, B. Mukherjee, P. Sharma, A. Pal, and H. J. Changlani, arXiv preprint arXiv:2212.13790 (2022).
- [42] J. M. Wahlen-Strothman, C. A. Jiménez-Hoyos, T. M. Henderson, and G. E. Scuseria, *Phys. Rev. B* **91**, 041114(R) (2015).
- [43] H. Nishimori and G. Ortiz, *Elements of phase transitions and critical phenomena* (Oup Oxford, 2010) p. 220.
- [44] M. E. Zhitomirsky and K. Ueda, *Phys. Rev. B* **54**, 9007 (1996).
- [45] S. Sachdev and R. N. Bhatt, *Phys. Rev. B* **41**, 9323 (1990).
- [46] L. Capriotti, F. Becca, A. Parola, and S. Sorella, *Phys. Rev. Lett.* **87**, 097201 (2001).